

Syncopated Dynamical Decoupling for Suppressing Crosstalk in Quantum Circuits

Bram Evert,¹ Zoe Gonzalez Izquierdo,^{2,3} James Sud,^{4,3} Hong-Ye Hu,^{2,3,*} Shon
Grabbe,² Eleanor G. Rieffel,² Matthew J. Reagor,^{1,†} and Zihui Wang^{2,3,‡}

¹*Rigetti Computing, Berkeley, CA[§]*

²*Quantum Artificial Intelligence Laboratory (QuAIL),
NASA Ames Research Center, Moffett Field, CA*

³*Research Institute for Advanced Computer Science (RIACS), USRA, Moffett Field, CA*

⁴*University of Chicago Computer Science Department, IL*

(Dated: March 13, 2024)

arXiv:2403.07836v1 [quant-ph] 12 Mar 2024

Abstract

Theoretically understanding and experimentally characterizing and modifying the underlying Hamiltonian of a quantum system is of utmost importance in achieving high-fidelity quantum gates for quantum computing. In this work, we explore the use of dynamical decoupling (DD) in characterizing undesired two-qubit couplings as well as the underlying single-qubit decoherence, and in suppressing them. We develop a syncopated dynamical decoupling technique which protects against decoherence and selectively targets unwanted two-qubit interactions, overcoming both significant hurdles to achieving precise quantum control and realizing quantum computing on many hardware prototypes. On a transmon-qubit-based superconducting quantum device, we identify separate white and $1/f$ noise components underlying the single-qubit decoherence and a static ZZ coupling between pairs of qubits. We suppress these errors using syncopated dynamical decoupling in two-qubit benchmarking experiments and significantly boost performance in a realistic algorithmic quantum circuit.

I. INTRODUCTION

Error suppression techniques play a crucial role in exploring applications of current noisy quantum hardware as well as in achieving error threshold for fault-tolerant quantum computing [1]. Among them, dynamical decoupling (DD) has emerged as a powerful strategy [2–10]. By applying a sequence of pulses to a qubit, DD engineers an effective Hamiltonian that averages out unwanted inter-qubit couplings or the qubit interaction with the environment [11]. With its simplicity in concept, design and implementation, and great versatility in application, DD has a long track record of successfully suppressing single-qubit decoherence on different quantum device types and noise of various power spectra [12, 13].

In this work, we take this approach a step further by designing and implementing DD sequences to measure and suppress an unwanted interaction between two qubits, while maintaining their power in mitigating single qubit decoherence. As an added benefit, our technique enables the characterization of this single-qubit decoherence.

* Presently at Harvard University.

† Presently at Google, Inc.

‡ zhihui.wang@nasa.gov

§ bevert@rigetti.com

Crosstalk [14] refers to an undesired effect on one qubit caused by the operation or existence of another qubit. It constitutes a great hurdle in achieving high-fidelity two-qubit gates and high fidelity in quantum circuits. In this study, we focus on eliminating ZZ crosstalk of the form $\exp[-i\theta ZZt]$, which results from the engineered system Hamiltonian in the transmon-qubit-based superconducting system, but the design principle generalizes to a broad family of two-body couplings. Prior work demonstrated that, for two qubits coupled in ZZ form, a periodic decoupling sequence applied to one qubit with the second qubit left idle, the ZZ effect on the second qubit will be averaged out [15, 16]. In Ref. [17] it was proposed that single-qubit DD be used to decouple crosstalk between a data qubit and idle qubits coupled to it. However, with identical periodic DD sequences applied to multiple qubits, the crosstalk among them remains. In this paper, we propose a scheme for scheduling decoupling pulses to target particular static couplings. We refer to this scheme as syncopated dynamical decoupling, borrowing a term from music which refers to the practice of playing a rhythm off-beat. The use of syncopation suppresses the crosstalk among an entire set of qubits with static couplings, rather than only a qubit of interest. Since syncopated DD also retains its mechanism of suppressing dephasing on single qubits, it protects all the qubits in the system and serves as a powerful approach for crosstalk detection and suppression in quantum systems.

II. SEQUENCE DESIGN FOR DYNAMICAL DECOUPLING

The theory of DD originated in the field of nuclear magnetic resonance (NMR) [11, 15, 18–23], as a way to enhance the coherence time of a collection of nuclear spins, by utilizing fast control pulse sequences to average out the effects of noise. Its development has been quickly gaining momentum thanks to the advances in quantum technology; the ability to precisely control individual qubits has allowed the use of DD to prolong their coherence time. A variety of DD sequences have been designed [13, 24–26] to target the noise spectra that arise for different physical realizations of qubits.

Our primary target in this study is a static coupling between qubits, we thus will focus on the operator aspect of the DD design, i.e., identifying a set of single-qubit operators (pulses) that has the potential of achieving a decoupled effective Hamiltonian. The Pauli operators are a complete set of orthogonal basis in the Hilbert space, and any Hermitian operator can

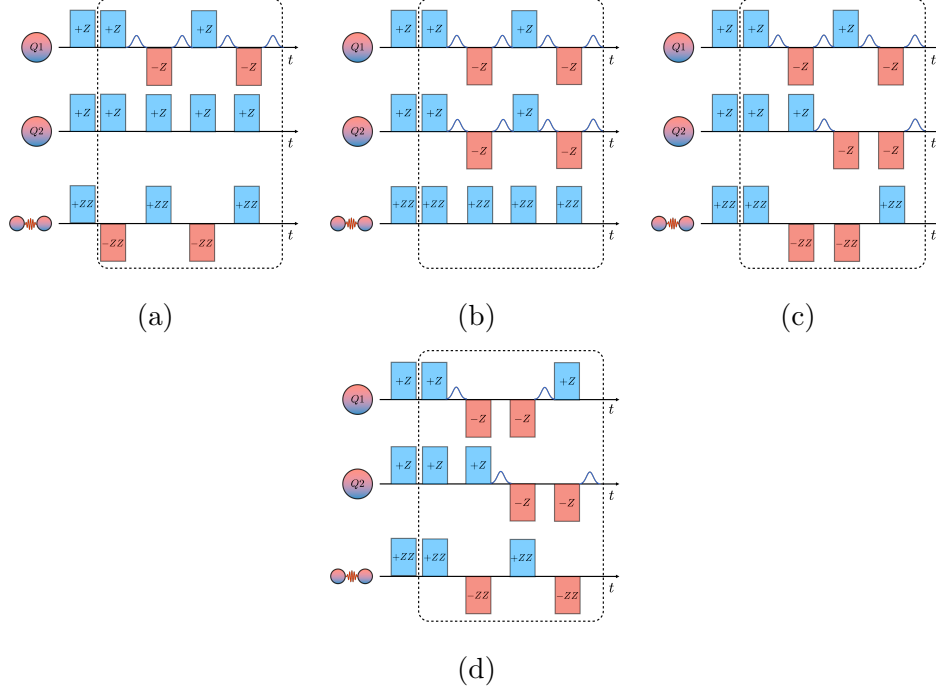


FIG. 1: Illustration of DD schemes (x, y) on a two-qubit system subject to a ZZ coupling. DD sequence x and y are applied to each qubit individually. **(a)** Scheme (XXXX, NONE).

Decoherence on the first qubit, as well as ZZ coupling, are canceled out by the DD sequence, while decoherence on the second qubit remains. **(b)** Synchronized DD Scheme (XXXX, XXXX). When the same sequence is applied to both qubits synchronously, individual decoherence is removed, but the ZZ coupling between them is unaffected. **(c)** Syncopated DD scheme (XXXX, XX). This scheme averages out ZZ coupling as well as single-qubit decoherence on both qubits. **(d)** Syncopated DD scheme (XX-CPMG, XX). Shifting one sequence can also achieve syncopation, with fewer pulses overall. The pulse duration is exaggerated for illustration purposes.

be represented as a vector using the Pauli basis. Given a Hermitian operator $A \in \mathbb{C}^{2 \times 2}$, it can be written as $A = \alpha I + \beta X + \gamma Y + \zeta Z$ or $|A\rangle\rangle = (\alpha, \beta, \gamma, \zeta)$ in the Pauli basis [27]. And any unitary quantum channel $\mathcal{C}_u[A] = UAU^\dagger$ can be represented as a unitary matrix \hat{U} in this basis, with its action represented as matrix multiplication, i.e. $\hat{U}|A\rangle\rangle$, which is also called superoperator representation. With this representation, the problem of DD sequence design is then translated into a matrix optimization problem. The goal for the search is to arrive at a zero vector for the targeted crosstalk term (corresponding to zero average Hamiltonian), by optimizing a binary matrix in Pauli basis with each input representing

whether to apply a specific operator. The theory is detailed in Appendix C.

For application convenience, we limit the DD sequence to be composed of only π -pulses (X or Y operators) as any such sequence can be natively implemented on superconducting qubit systems with a single microwave pulse. For a variety of Hamiltonian terms we tried as crosstalk, the matrix search always output pulse schemes that achieve the decoupling of these terms, see Appendix C for some examples. We identify a family of *syncopated* DD sequences capable of decoupling the ZZ crosstalk that is the focus of this study. We describe in detail two approaches of achieving syncopation. For a two qubit system, the “frequency multiplication” syncopation, as proposed in Ref. [28], applies a periodic DD pulse sequence to each qubit, but the number of pulses on one qubit is an even multiplier of the other. This is illustrated in Fig. 1c, where we show the (XXXX, XX) scheme; in a “shifted” syncopation scheme, (XX-CPMG, XX), two pulses are applied to each qubit in an off-beat fashion, as illustrated in Fig. 1d. The shifted scheme is optimal in the number of pulses.

We illustrate how such syncopated DD sequences remove ZZ as well as suppress single qubit dephasing by observing the phase accumulation on each qubit, in comparison with the synchronized DD (see Fig. 1b) and neighbor only DD (see Fig. 1a) which only removes part of the noise terms. These DD sequences will also be carried out and compared in our benchmarking experiments and discussed throughout the paper.

III. RESULTS

In the Rigetti Aspen architecture [29], two transmon qubits are connected by a fixed capacitive coupler, which leads to an effective ZZ term between the pair [30]. The coupling is necessary for 2-qubit gate operation, but remains present while qubits are idling and leads to an unwanted term in the Hamiltonian. Since the source of the coupling is a physical capacitance on the chip, it can be relied on to be static over both the timescale of experiments and the lifetime of the chip. This known source of static crosstalk provides a testbed to apply syncopated dynamical decoupling.

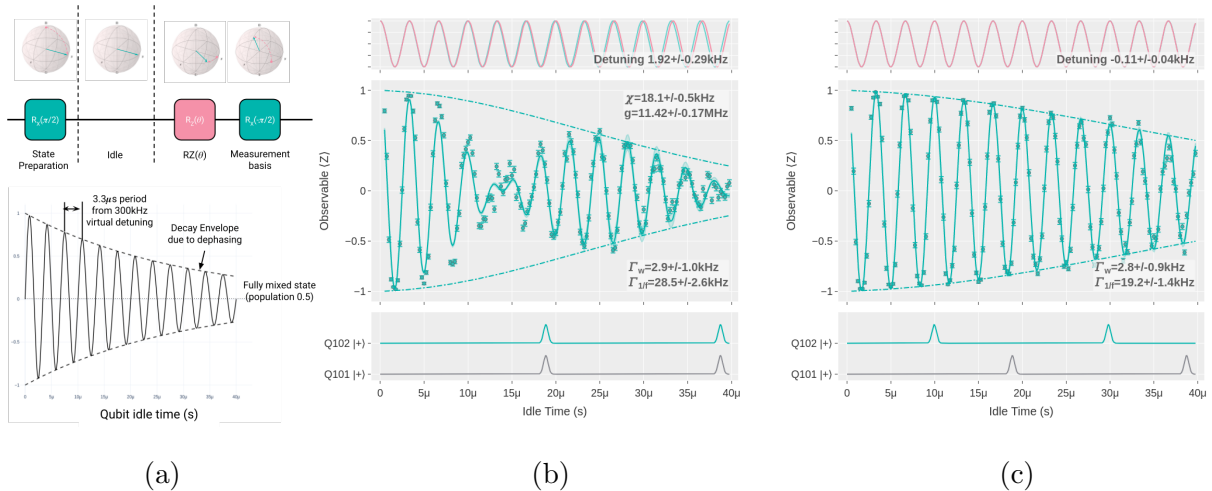


FIG. 2: The experimental setup is shown in (a). The qubit is prepared in the $|+\rangle$ state, remains there for some idle time, in which a decoupling sequence is applied, and undergoes the pre-measurement rotation. The result should be a characteristic Ramsey decay curve, where the physical detuning can be extracted from the frequency of the oscillation and the dephasing rate can be extracted from the envelope. When the neighbour is in the (b) $|+\rangle$ state, the detuning is negligible but a characteristic beating frequency of 18.1Khz is visible. With the (c) syncopated DD sequences, the characteristic beating is suppressed and we recover the expected curve. The $\Gamma_{1/f}$ dephasing rate is reduced from 28.5kHz to 19.2kHz, indicating improved protection from decoherence.

A. Benchmarking: Measuring and mitigating crosstalk in a two-qubit system

Being able to precisely measure the ZZ coupling magnitude not only helps understand low-level qubit physics and informs hardware design, but also can inform tailoring of error suppression techniques applied to quantum circuits. We begin by applying dynamical decoupling sequences designed to first, measure the magnitude of a static ZZ coupling and, second, suppress it on the pair of qubits.

1. Measuring decoherence

In order to study the decoherence on individual qubits, we make use of Ramsey T_2^* experiments [31]. In these experiments, a qubit is prepared in a superposition state, typically

$|+\rangle$ or $|i\rangle$, followed by an idle time during which the qubit is subject to noise and (if applied) DD. Finally, a Z-rotation proportional to the idle time is applied, implementing a “virtual detuning”, and the resulting state is projected onto the measurement axis with the inverse of the preparation operator. The circuit and expected decay is pictured in Fig. 2a. To obtain a reliable fitting of Eq. (1), we set a virtual detuning of $\omega_0 = 300\text{kHz}$, which is about an order of magnitude faster than the physical detunings and allows us to resolve dozens of oscillations in our expected dephasing times of 10-100 μs .

The resulting curve without DD can be described by evolution of the expected value

$$\langle Z(t) \rangle = e^{-\Gamma_w t} e^{-\Gamma_{1/f}^2 t^2} \cos [(\omega_0 + \delta\omega)t], \quad (1)$$

where $\delta\omega$ is the physical detuning and ω_0 is an introduced virtual detuning. The two decay factors are the empirical decoherence form that prevails on the hardware, an exponential decay due to white noise and stretched exponential decay due to $1/f$ -noise, at a decay rate Γ_w and $\Gamma_{1/f}$, respectively [32]. The observable, $\langle Z(t) \rangle$, is calculated upon measurement in the Z basis. In these experiments, readout mitigation is applied using the method of Ref. [33].

2. Demonstrating and measuring the effect of ZZ coupling

We then examine the idle crosstalk between two qubits. The two qubits are initiated in $|+\rangle \otimes |+\rangle$ state, and the observable value of each qubit in a Ramsey experiment is examined. Synchronized DD is applied to the pair, meaning that each qubit experiences precisely the same schedule of decoupling pulses. The decoupling pulses ensure that the crosstalk effect of other nearby qubits is eliminated, but any ZZ coupling between the pair remains, as illustrated in Fig 1b.

Adding the effect of a ZZ coupling J to the model described by Eq. (1), we expect the observable to evolve according to

$$\langle Z(t) \rangle = e^{-\Gamma_w t} e^{-\Gamma_{1/f}^2 t^2} \cos [(\omega_0 + \delta\omega)t] \cos \left(\frac{J}{2} t \right), \quad (2)$$

where the decay factors similar to those in Eq. (1) account for the single-qubit decoherence under single-qubit DD, and the rest is derived from the quantum evolution of the initial

state under the Hamiltonian

$$H = JZ_1Z_2 + (\omega_0 + \delta\omega)Z_1. \quad (3)$$

The ZZ crosstalk between the qubit pair manifests as a beating in the Ramsey measurement, at a frequency proportional to the crosstalk magnitude, J . Such beating is observed experimentally, see Fig. 2b. Due to this beating, the system undergoes a rapid loss of fidelity far exceeding the simple dephasing rate. Eq. (2) also provides an efficient way of measuring the crosstalk. By fitting the data into the equation with fitting parameters $\delta\omega$, Γ_ω , $\Gamma_{1/f}$, $\delta\omega$ and J , we obtain the two decoherence rates, the residual physical detuning, and the crosstalk magnitude, J . A pair of highly detuned transmon qubits coupled by a fixed capacitance gives rise to state-dependent frequency shifts, sometimes referred to as the dispersive shift, χ . The observed beating frequency, J , can be related to the dispersive shift and thus the bare qubit-qubit coupling, g , using Eq. (4), where f is the qubit frequency, η is the qubit anharmonicity and the qubits are labeled by subscripts 0 and 1. We direct readers to [30] for a full treatment.

$$\chi = \frac{2g^2(\eta_0 + \eta_1)}{(f_0 - f_1 + \eta_1)(f_0 - f_1 - \eta_1)}, \quad (4)$$

χ is 2 times the measured beating frequency and is equivalent to J in Eq. (1) and (3).

The bare qubit-qubit coupling, g , is directly proportional to the capacitance between the two transmons, g_C , and is thus a hardware design parameter which must be carefully controlled. Engineering the strength of g is critical as it determines the speed of two-qubit gates and precise measurements are important for select gate operating points, constructing a physical model of the device and providing feedback for quantum circuit designers.

Using the average of our synchronized DD Ramsey measurements, we extract a beating frequency $\chi = 35.6 \pm 1.8$ kHz. This is consistent with the ZZ coupling extracted by measuring the difference in physical detuning caused by preparing the neighboring qubits in $|0\rangle$ and $|1\rangle$ states (39.1 ± 0.3 kHz). This corresponds to a value of 11.34 ± 0.28 MHz for g , which is consistent with the designed capacitance and matches the value of g extracted from the 2-qubit gate operating point as described in Appendix D [30]. We thus note that synchronized decoupling sequences can serve as a viable method for probing the qubit-qubit coupling magnitude on hardware or providing a starting guess for 2-qubit gate bringup.

Our protocol of measuring the crosstalk using synchronized DD is similar in spirit to the JAZZ protocol where often a spin echo induced by a single pulse is applied to both qubits to decouple the system from surrounding qubits [15, 34, 35], however it differs by using only a single preparation state, and a variety of sequence designs. We suggest that with careful design of sequences, the richness of synchronized decoupling sequences can offer a diagnostic tool for measuring known and unintended coupling strengths that can be tailored to the specific noise environment.

It is a common practice to characterize the dephasing time under the assumption that the T_2 decay follows a single exponential. However, if the Ramsey experiments in our study were fit into a single exponential decay, the fitting curve would clearly deviate from the experimental data beyond certain time. Such a feature is consistent through all experiments. The data are fit much better by also including $1/f$ noise in the model. We thus note that our benchmark experiments also provide an efficient tool to probe and characterize single-qubit noise and its underlying physics.

3. *Mitigating the effect of ZZ coupling*

While we have shown that dynamical decoupling can be used to isolate and measure the effect of ZZ coupling, during normal operation of the QPU it is desirable to eliminate this unintended effect. To this end, we introduce the syncopated decoupling scheme (Figs. 1c and 1d).

To demonstrate the scheme, we repeat the experiment shown in Fig. 2b, but with syncopated, rather than synchronized, pulses. The results are shown in Fig. 2c. In this case, we achieve syncopation by shifting the relative timing of the DD sequences (as depicted in Fig. 1d), but using the frequency doubling approach (Fig. 1c) yields similar results (see Appendix B). The suppression of the ZZ crosstalk is evidenced by the elimination of the beating pattern, and the recovery of the expected Ramsey decay envelope. Experimental results with a set of different initial states is shown in Appendix B, where we observe that the physical detuning caused by the state of the neighbouring qubit is also eliminated.

The experiment is repeated for wide range of DD sequence combinations and qubit states. The full results can be found in Appendix B and are summarized in Table I. We observe that syncopated decoupling suppresses the physical detuning, eliminates the beating caused

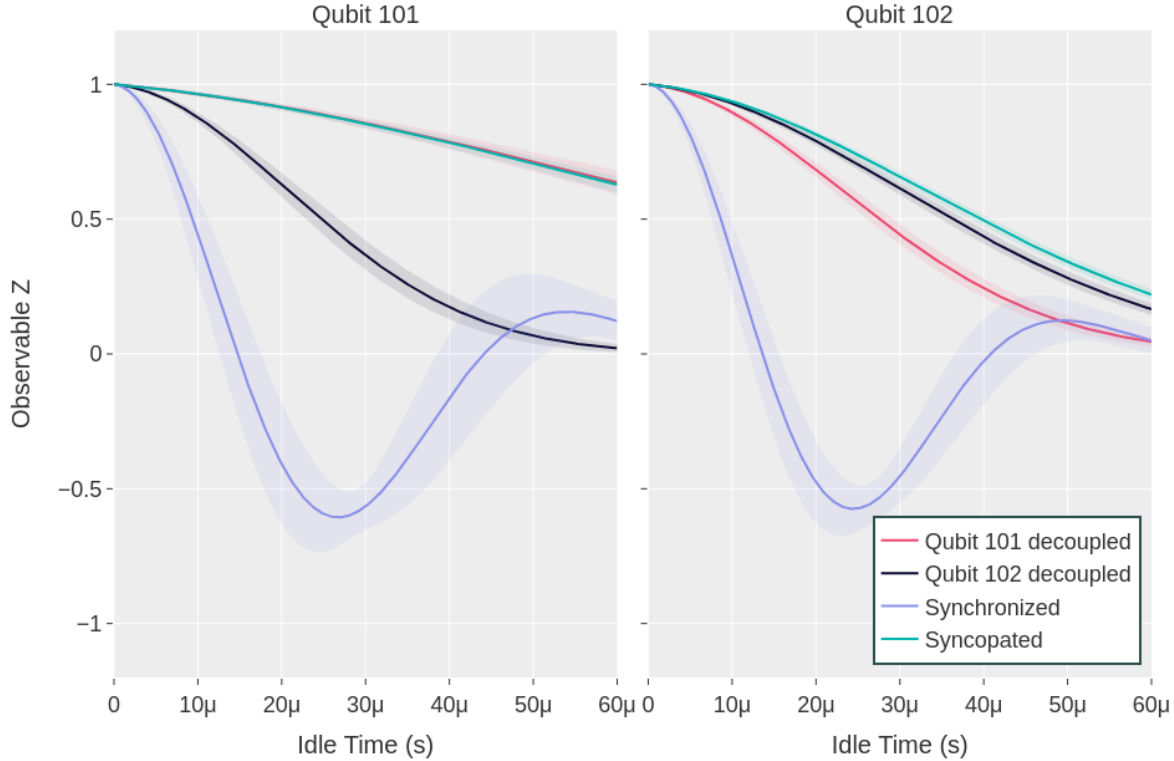


FIG. 3: The average decay envelope of each qubit when different DD schemes are applied.

DD applied to Qubit 101 alone is shown in red, to Qubit 102 alone is shown in black.

Synchronized and syncopated DD are shown in blue and teal, respectively. The error bands reflect the standard error of the parameter estimate over the set of experiments.

The syncopated DD provides the best protection to both qubits.

by the crosstalk, and suppresses the $1/f$ dephasing rate, enhancing the coherent time.

The efficacy of the syncopated DD is highlighted by examining the decay envelopes measured for the different decoupling schemes for both qubits, as in Fig. 3. While decoupling one qubit only suppresses its dephasing rate and the crosstalk, the neighbouring qubit is still subjected to dephasing. When the same decoupling sequence is applied to both qubits in a synchronized manner, the beating of the decay envelope from the crosstalk indicates the presence of a large coherent error. By syncopating the decoupling sequences, decoherence on both qubits is simultaneously suppressed along with the crosstalk.

B. Application of Syncopated DD to algorithmic circuits

Applying dynamical decoupling to improve the performance of application circuits can be non-trivial. A typical approach is to inspect the compiled circuit, locate idling periods of qubits in the circuit and insert the DD sequence of choice [36, 37]. However, as demonstrated in Sec. III A, synchronized DD applied to a pair of idle qubits can lead to a perverse outcome where a static coupling remains. To demonstrate the efficacy of our syncopated DD, we constructed a Quantum Alternating Operator Ansatz (QAOA) circuit [38] that aims to solve the MAXCUT problem on a 4-qubit square as an example.

To minimize the detrimental effect of two-qubit gate infidelity, we implement a level-one QAOA algorithm, with the optimal angles determined theoretically [39]. The algorithm is then composed of state preparation, a layer of phase-separators followed by a layer of single-qubit mixing operators, and a final measurement, as shown in Fig. 4. We focus on the subroutine of the phase-separation layer, which can be further decomposed into a two qubit native gate on each edge. On the Rigetti Aspen architecture, neighbouring 2-qubit gates are typically not executed simultaneously to minimize operational crosstalk. In the case of our square lattice, this naturally leads to a pair of idle qubits in the circuit while the phase-separator is applied to the other two. The phase separator is implemented using the native CPHASE gate of duration 200ns, The $RX(\pi)$ gates that compose the X pulses in DD are calibrated to a duration of 40ns, which means we can fit up to 4 decoupling pulses within the idle time. As entangling gate times are reduced, we expect that the importance of using sequences with minimal number of pulses will grow. We discuss in Appendix C 1 how syncopation can be applied to more complex scenarios.

The results of the experiment are shown in the bottom portion of Fig. 4. A common figure of merit in QAOA is the approximation ratio, which is the fraction of the true best cost found by the algorithm. However, in this experiment we wish to probe the effect of noise on the QPU, so we define the “performance ratio” as the fraction of the noisy divided by the noiseless approximation ratio, which is directly related to the circuit fidelity. Thus, if the QPU were error-free we would report a performance ratio of 1, while a QPU subject to strong depolarizing noise would have a performance ratio of 0. Implementing the bare circuit (i.e. with no error mitigation) results in a low performance ratio, due to readout errors (3% - 8%), 1q and 2q gate errors (4% and 10%), decoherence and crosstalk. Our syncopated

dynamical decoupling scheme mitigates the effects of crosstalk errors and decoherence on the idle qubits, and significantly boosts the performance, as shown in the bottom left panel of Fig. 4. In order to further mitigate the effects of coherent errors and state-dependent errors, we introduce the use of random compilation [40]. The use of randomized compiling prevents coherent errors from accumulating, which can improve circuit fidelity. In addition, it ensures that the fidelity improvement is robust under many logically equivalent instances of the circuit. Applying syncopated DD on top of random compilation further doubled the performance ratio, as shown in the bottom right panel of Fig. 4. These two techniques hence not only are compatible with each other, but simultaneously contribute to improving the performance ratio of the circuit.

ACKNOWLEDGMENTS

The work described in Sec. III A was supported by the Defense Advanced Research Projects Agency (DARPA) under Agreement No. HR00112090058. The work in Sec. III B was supported by the U.S. Department of Energy, Office of Science, National Quantum Information Science Research Centers, Superconducting Quantum Materials and Systems Center (SQMS) under the contract No. DE-AC02-07CH11359 through NASA-DOE SAA 403602. We are grateful for support from NASA Ames Research Center. Z.G.I. and Z.W. are supported by NASA Academic Mission Services (NAMS), contract number NNA16BD14C.

-
- [1] D. Gottesman, An Introduction to Quantum Error Correction and Fault-Tolerant Quantum Computation, arXiv e-prints , arXiv:0904.2557 (2009), arXiv:0904.2557 [quant-ph].
 - [2] L. Viola and S. Lloyd, Dynamical suppression of decoherence in two-state quantum systems, *Phys. Rev. A* **58**, 2733 (1998).
 - [3] L. Viola, E. Knill, and S. Lloyd, Dynamical decoupling of open quantum systems, *Phys. Rev. Lett.* **82**, 2417 (1999).
 - [4] L. Viola, S. Lloyd, and E. Knill, Universal control of decoupled quantum systems, *Phys. Rev. Lett.* **83**, 4888 (1999).
 - [5] P. Zanardi, Symmetrizing evolutions, *Physics Letters A* **258**, 77 (1999).

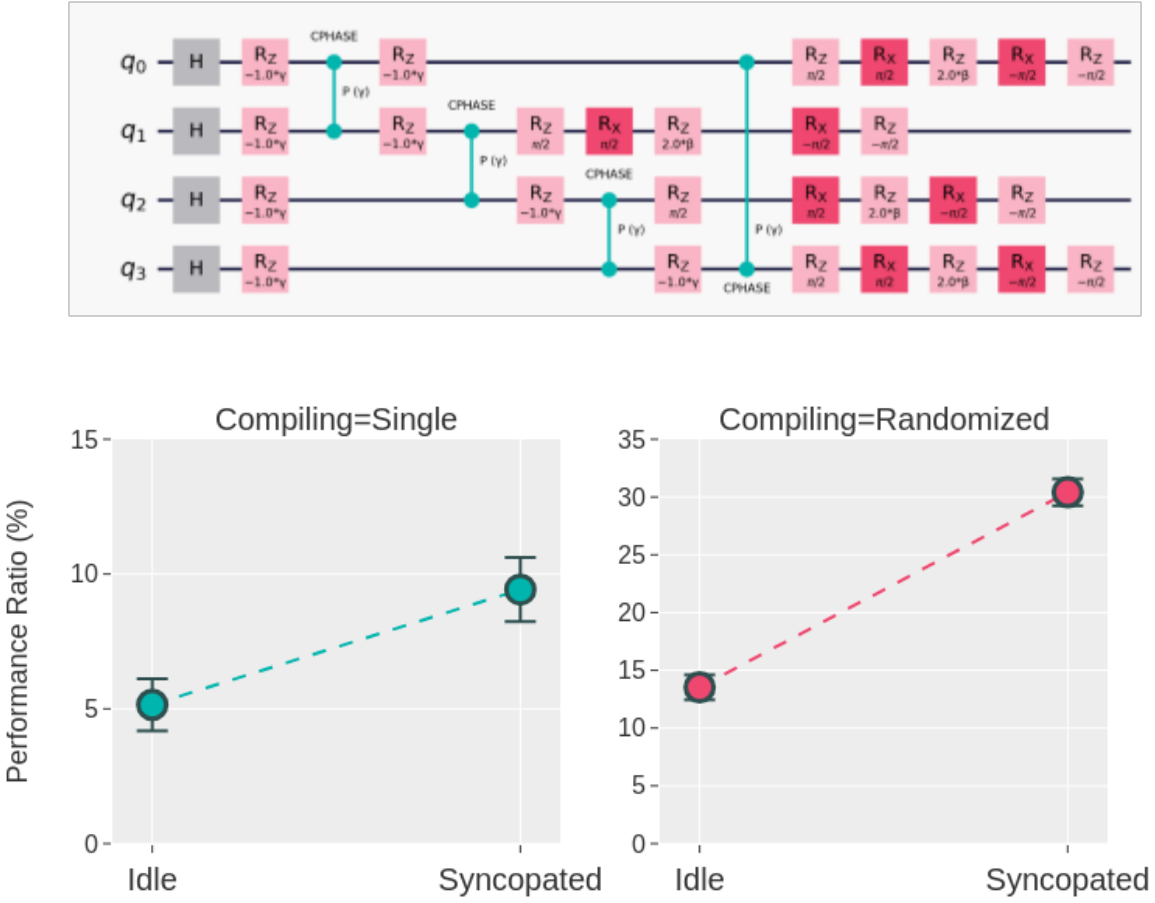


FIG. 4: (top) A level-1 QAOA circuit was executed to approximate the MAXCUT of a square graph with and without error mitigation applied. The performance ratio (bottom) is shown for the circuit with the qubits left idle and with syncopated dynamical decoupling applied. Bottom right: Syncopated dynamical decoupling is combined with randomized compiling. Applying syncopated DD improves performance with or without randomized compiling, and using the two error mitigation methods in conjunction provides the most remarkable improvement.

- [6] D. Vitali and P. Tombesi, Using parity kicks for decoherence control, *Phys. Rev. A* **59**, 4178 (1999).
- [7] L.-A. Wu, M. S. Byrd, and D. Lidar, Efficient universal leakage elimination for physical and encoded qubits, *Physical review letters* **89**, 127901 (2002).

- [8] K. Khodjasteh and D. A. Lidar, Fault-tolerant quantum dynamical decoupling, *Phys. Rev. Lett.* **95**, 180501 (2005).
- [9] M. J. Biercuk, H. Uys, A. P. VanDevender, N. Shiga, W. M. Itano, and J. J. Bollinger, Optimized dynamical decoupling in a model quantum memory, *Nature* **458**, 996 (2009).
- [10] A. M. Souza, G. A. Álvarez, and D. Suter, Robust dynamical decoupling, *Philosophical Transactions of the Royal Society A: Mathematical, Physical and Engineering Sciences* **370**, 4748 (2012).
- [11] J. S. Waugh, C. H. Wang, L. M. Huber, and R. L. Vold, Multiple-Pulse NMR Experiments, *The Journal of Chemical Physics* **48**, 662 (1968), https://pubs.aip.org/aip/jcp/article-pdf/48/2/662/11001729/662_1_online.pdf.
- [12] G. A. Álvarez and D. Suter, Measuring the spectrum of colored noise by dynamical decoupling, *Phys. Rev. Lett.* **107**, 230501 (2011).
- [13] P. Szańkowski, G. Ramon, J. Krzywda, D. Kwiatkowski, and Ł. Cywiński, Environmental noise spectroscopy with qubits subjected to dynamical decoupling, *Journal of Physics Condensed Matter* **29**, 333001 (2017), arXiv:1705.02262 [cond-mat.mes-hall].
- [14] M. Sarovar, T. Proctor, K. Rudinger, K. Young, E. Nielsen, and R. Blume-Kohout, Detecting crosstalk errors in quantum information processors, *Quantum* **4**, 321 (2020).
- [15] J. Garbow, D. Weitekamp, and A. Pines, Bilinear rotation decoupling of homonuclear scalar interactions, *Chemical Physics Letters* **93**, 504 (1982).
- [16] B. Pokharel, N. Anand, B. Fortman, and D. A. Lidar, Demonstration of fidelity improvement using dynamical decoupling with superconducting qubits, *Phys. Rev. Lett.* **121**, 220502 (2018).
- [17] V. Tripathi, H. Chen, M. Khezri, K.-W. Yip, E. Levenson-Falk, and D. A. Lidar, Suppression of crosstalk in superconducting qubits using dynamical decoupling, *Physical Review Applied* **18**, 10.1103/physrevapplied.18.024068 (2022).
- [18] E. L. Hahn, Spin echoes, *Phys. Rev.* **80**, 580 (1950).
- [19] H. Y. Carr and E. M. Purcell, Effects of diffusion on free precession in nuclear magnetic resonance experiments, *Phys. Rev.* **94**, 630 (1954).
- [20] S. Meiboom and D. Gill, Modified Spin-Echo Method for Measuring Nuclear Relaxation Times, *Review of Scientific Instruments* **29**, 688 (1958).
- [21] J. S. Waugh, L. M. Huber, and U. Haeberlen, Approach to high-resolution nmr in solids, *Phys. Rev. Lett.* **20**, 180 (1968).

- [22] J. Waugh, Theory of broadband spin decoupling, *Journal of Magnetic Resonance* (1969) **50**, 30 (1982).
- [23] L. M. K. Vandersypen and I. L. Chuang, Nmr techniques for quantum control and computation, *Rev. Mod. Phys.* **76**, 1037 (2005).
- [24] A. Maudsley, Modified carr-purcell-meiboom-gill sequence for nmr fourier imaging applications, *Journal of Magnetic Resonance* (1969) **69**, 488 (1986).
- [25] T. Gullion, D. B. Baker, and M. S. Conradi, New, compensated carr-purcell sequences, *Journal of Magnetic Resonance* (1969) **89**, 479 (1990).
- [26] M. J. Biercuk, A. C. Doherty, and H. Uys, Dynamical decoupling sequence construction as a filter-design problem, *Journal of Physics B: Atomic, Molecular and Optical Physics* **44**, 154002 (2011).
- [27] One should notice that the basis is not normalized. It can be normalized by assigning a prefactor of $1/\sqrt{D}$ where D is the Hilbert space dimension.
- [28] G. A. Paz-Silva, S.-W. Lee, T. J. Green, and L. Viola, Dynamical decoupling sequences for multi-qubit dephasing suppression and long-time quantum memory, *New Journal of Physics* **18**, 073020 (2016).
- [29] S. A. Caldwell, N. Didier, C. A. Ryan, E. A. Sete, A. Hudson, P. Karalekas, R. Manenti, M. P. da Silva, R. Sinclair, E. Acala, N. Alidoust, J. Angeles, A. Bestwick, M. Block, B. Bloom, A. Bradley, C. Bui, L. Capelluto, R. Chilcott, J. Cordova, G. Crossman, M. Curtis, S. Deshpande, T. E. Bouayadi, D. Girshovich, S. Hong, K. Kuang, M. Lenihan, T. Manning, A. Marchenkov, J. Marshall, R. Maydra, Y. Mohan, W. O'Brien, C. Osborn, J. Otterbach, A. Papageorge, J.-P. Paquette, M. Pelstring, A. Polloreno, G. Prawiroatmodjo, V. Rawat, M. Reagor, R. Renzas, N. Rubin, D. Russell, M. Rust, D. Scarabelli, M. Scheer, M. Selvanayagam, R. Smith, A. Staley, M. Suska, N. Tezak, D. C. Thompson, T.-W. To, M. Vahidpour, N. Vodrahalli, T. Whyland, K. Yadav, W. Zeng, and C. Rigetti, Parametrically activated entangling gates using transmon qubits, *Phys. Rev. Appl.* **10**, 034050 (2018).
- [30] N. Didier, E. A. Sete, M. P. da Silva, and C. Rigetti, Analytical modeling of parametrically-modulated transmon qubits, *Physical Review A* **97**, 022330 (2018), arXiv:1706.06566 [cond-mat, physics:quant-ph].
- [31] I. Chiorescu, Y. Nakamura, C. J. P. M. Harmans, and J. E. Mooij, Coherent Quantum Dynamics of a Superconducting Flux Qubit, *Science* **299**, 1869 (2003), arXiv:cond-mat/0305461

[cond-mat.mes-hall].

- [32] J. Bylander, S. Gustavsson, F. Yan, F. Yoshihara, K. Harrabi, G. Fitch, D. G. Cory, Y. Nakamura, J.-S. Tsai, and W. D. Oliver, Noise spectroscopy through dynamical decoupling with a superconducting flux qubit, *Nature Physics* **7**, 565 (2011).
- [33] B. Nachman, M. Urbanek, W. A. de Jong, and C. W. Bauer, Unfolding quantum computer readout noise, *npj Quantum Information* **6**, 84 (2020), zSCC: 0000029.
- [34] J. Ku, X. Xu, M. Brink, D. McKay, J. Hertzberg, M. Ansi, and B. Plourde, Suppression of unwanted zz interactions in a hybrid two-qubit system, *Physical Review Letters* **125**, 200504 (2020).
- [35] R. Sagastizabal, S. P. Premaratne, B. A. Klaver, M. A. Rol, V. Negîrneac, M. Moreira, X. Zou, S. Johri, N. Muthusubramanian, M. Beekman, C. Zachariadis, V. P. Ostroukh, N. Haider, A. Bruno, A. Y. Matsuura, and L. DiCarlo, Variational preparation of finite-temperature states on a quantum computer (2020), arXiv:2012.03895 [quant-ph] version: 1.
- [36] S. Niu and A. Todri-Sanial, Analyzing strategies for dynamical decoupling insertion on ibm quantum computer, arXiv **2022**, 10.48550/arXiv.2204.14251 (2022).
- [37] Qiskit contributors, Qiskit: An open-source framework for quantum computing (2023).
- [38] S. Hadfield, Z. Wang, B. O’Gorman, E. G. Rieffel, D. Venturelli, and R. Biswas, From the quantum approximate optimization algorithm to a quantum alternating operator ansatz, *Algorithms* **12**, 10.3390/a12020034 (2019).
- [39] Z. Wang, S. Hadfield, Z. Jiang, and E. G. Rieffel, Quantum approximate optimization algorithm for maxcut: A fermionic view, *Phys. Rev. A* **97**, 022304 (2018).
- [40] J. J. Wallman and J. Emerson, Noise tailoring for scalable quantum computation via randomized compiling, *Phys. Rev. A* **94**, 052325 (2016), publisher: American Physical Society.
- [41] One could also generalize the theory for non-constant crosstalks and non-unitary channels with superoperator representation.
- [42] J. Choi, H. Zhou, H. S. Knowles, R. Landig, S. Choi, and M. D. Lukin, Robust dynamic hamiltonian engineering of many-body spin systems, *Phys. Rev. X* **10**, 031002 (2020).
- [43] T. Tsunoda, G. Bhole, S. A. Jones, J. A. Jones, and P. J. Leek, Efficient Hamiltonian programming in qubit arrays with nearest-neighbour couplings, *Physical Review A* **102**, 032405 (2020), arXiv:2003.07815 [quant-ph].
- [44] G. Bhole, T. Tsunoda, P. J. Leek, and J. A. Jones, Rescaling interactions for quantum control,

Physical Review Applied **13**, 034002 (2020), arXiv:1911.04806 [quant-ph].

- [45] S. Skiena, *Implementing Discrete Mathematics: Combinatorics and Graph Theory with Mathematics* (Addison-Wesley Longman Publishing Co., Inc., USA, 1991).

Appendix A: Detail on syncopation and related schemes

Consider an individual qubit experiencing dephasing (represented by a static Z error). If we apply an even number of π pulses about an axis in the x - y plane periodically, at the end of the DD sequence all the Z errors can be shown to cancel out. Furthermore, if we consider a neighboring qubit (like in Fig. 1a), which might be causing ZZ coupling with the original qubit, this ZZ coupling is also averaged out by the XXXX sequence applied to the first qubit. This was experimentally demonstrated in [16]. Such techniques for suppressing ZZ date back to early NMR literature. For example, in Ref. [15] a bilinear rotation decoupling (BIRD) sequence was proposed where, through pulse manipulation of a spin of a particular variety, an effective π -pulse could be induced on the subset of spins directly coupled to it, and decoupled the ZZ between the subset and the rest of spins. Recent work in the qubit context implemented a similar protocol where the π pulses were achieved with single-qubit controls and demonstrated its effectiveness experimentally. [17]

However, a drawback of this design is that the neighboring qubit is still subject to single-qubit decoherence. If the same DD sequence is applied to both qubits in a synchronized manner to mitigate individual decoherence, the ZZ crosstalk will not be averaged out, as shown in Fig. 1b. In a circuit where all qubits are data qubits, it would be more desirable to have a DD sequence that both suppresses decoherence and cancels out the crosstalk between all pairs of qubits.

One way to accomplish this is via “even multiplier frequency” DD sequences, in which a periodic DD pulse sequence is applied to each qubit of a pair, but the number of pulses applied to one is an even multiplier of the number applied to the other. This is illustrated in Fig. 1c, where we show the XXXX, XX sequence; while 4 pulses are applied to the first qubit, only 2 are applied to the second, at half the frequency.

TABLE I: The fit parameters for the experiments are summarized for syncopated and synchronized decoupling sequences where the neighbour is in state $|0\rangle$ or $|1\rangle$. We observe that with syncopation, the detuning is eliminated, and the $1/f$ decay rate is suppressed.

The reported parameters are the average of all the experiments performed.

Qubit	Decoupling	Neighbour	Detuning (kHz)	Γ_w (kHz)	$\Gamma_{1/f}$ (kHz)
101	Synchronized	$ 0\rangle$	-18.93 \pm 0.29	2.8 \pm 0.4	22.0 \pm 0.9
101	Synchronized	$ 1\rangle$	19.45 \pm 0.30	2.78 \pm 0.23	21.6 \pm 0.8
101	Syncopated	$ 0\rangle$	-0.71 \pm 0.06	2.79 \pm 0.20	9.0 \pm 0.5
101	Syncopated	$ 1\rangle$	0.90 \pm 0.05	2.79 \pm 0.24	8.2 \pm 0.5
102	Synchronized	$ 0\rangle$	-19.75 \pm 0.30	2.8 \pm 0.4	26.0 \pm 0.8
102	Synchronized	$ 1\rangle$	20.02 \pm 0.30	2.9 \pm 0.5	26.1 \pm 0.8
102	Syncopated	$ 0\rangle$	-0.103 \pm 0.035	2.79 \pm 0.21	19.2 \pm 0.5
102	Syncopated	$ 1\rangle$	0.403 \pm 0.033	2.79 \pm 0.23	18.8 \pm 0.5

Appendix B: More results on benchmarking: neighboring qubit in $|0\rangle$ and $|1\rangle$ states

In Sec. III A, we presented results for two qubit initialized in the $|++\rangle$ state, where the ZZ crosstalk manifested as a beating in the Ramsey oscillation. Here we show that our protocol is equally valid for initial states $|+0\rangle$ and $|+1\rangle$, where the physical detuning of a qubit is modulated by the state of its neighbour. Again, in order to isolate the pair of interest from others, we apply synchronized decoupling pulses to both qubits. The ZZ coupling between them results in the qubit frequency being dependent on the state of the neighbouring qubit, and we thus observe a detuning of ± 20 kHz conditioned on the state of the neighbour, shown in Fig. 7.

Appendix C: Extending Syncopation

While our experiments focus on decoupling the static ZZ coupling which is present on the hardware, in principle we can target any static coupling using syncopation. On superconducting platforms, we typically have only physical X and Y pulses available. The syncopation matrix in Table II summarizes which X and Y pulse-based sequences eliminate

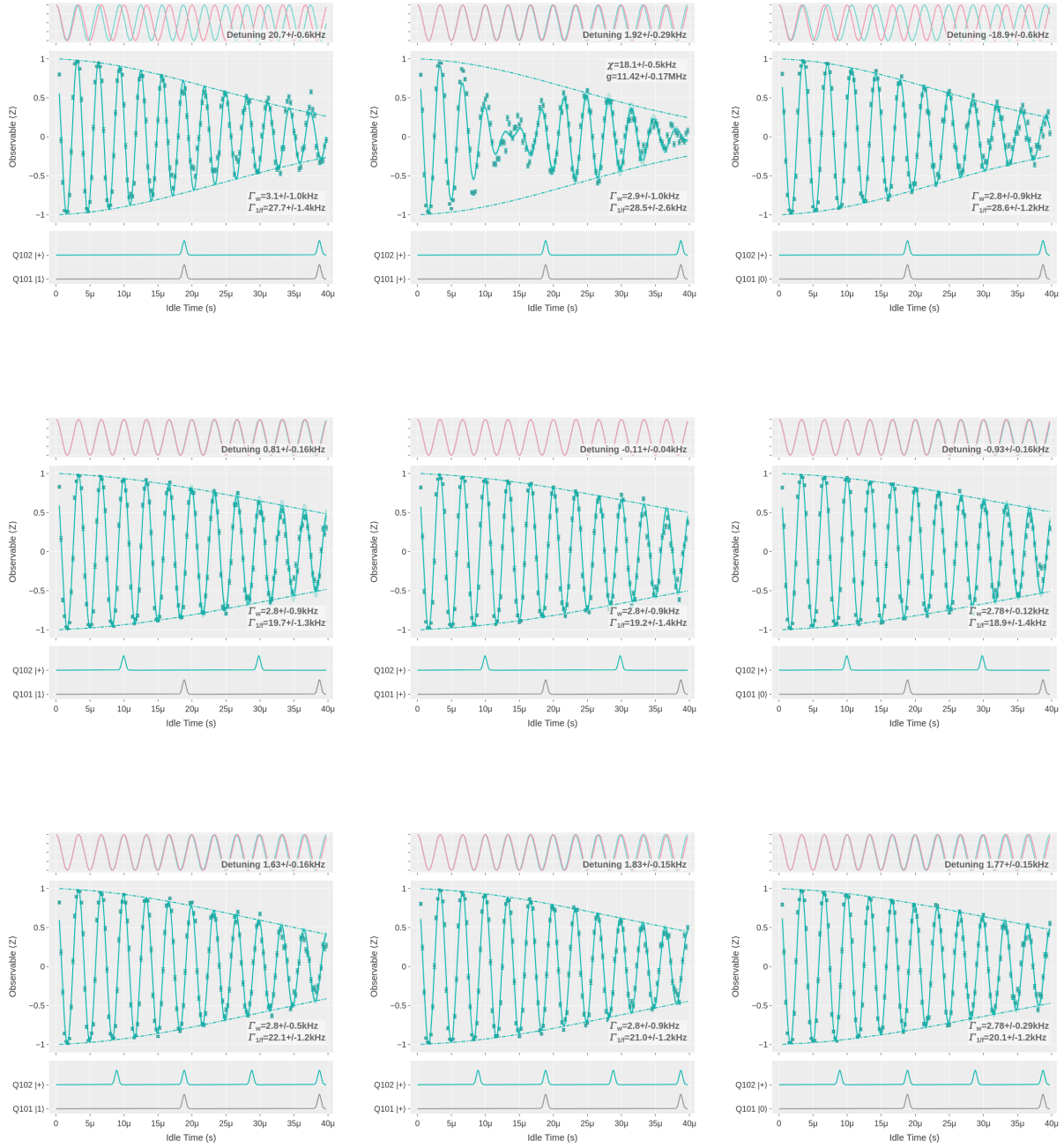


FIG. 5: (Top row) When neighbouring qubit 101 is in the (a) $|1\rangle$ state, qubit 102 experiences a physical detuning of +20.7kHz. When the neighbour is in the (b) $|i\rangle$ state, the detuning is negligible but a characteristic beating frequency of 18.1Khz is visible. When the neighbour is in the (c) $|0\rangle$ state, qubit 102 experiences a physical detuning of -18.9kHz. The detunings and beating frequency correspond to a g of 11.42 MHz. (Middle row) With the time-shifted syncopated DD sequences, the detuning is eliminated in all cases, and the characteristic beating is suppressed. The decay envelopes are also more gradual, indicating an improved protection from decoherence. (Bottom row) The

frequency-doubled syncopated sequences show similar results.

TABLE II: The syncopation matrix identifies which sequences syncopate with each other, for the XX , YY or ZZ static couplings up to length 4.

Qubit 1 Sequence	XX	XX-CPMG	XXXX	XXXX-CPMG	YXYX	YXYX-CPMG	YXYX	YXYX-CPMG	YY	YY-CPMG	YYYY	YYYY-CPMG
Qubit 0 Sequence												
XX		YY, ZZ	YY, ZZ	YY, ZZ	XX, YY, ZZ	XX, ZZ	XX, ZZ	XX, ZZ	XX, YY	XX, YY, ZZ	XX, YY, ZZ	XX, YY, ZZ
XX-CPMG	YY, ZZ		YY, ZZ	YY, ZZ	XX, ZZ	XX, ZZ	XX, YY, ZZ	XX, ZZ	XX, YY, ZZ	XX, YY	XX, YY, ZZ	XX, YY, ZZ
XXXX	YY, ZZ	YY, ZZ		YY, ZZ	XX, YY	XX, YY, ZZ	XX, YY	XX, YY, ZZ	XX, YY, ZZ	XX, YY, ZZ	XX, YY	XX, YY, ZZ
XXXX-CPMG	YY, ZZ	YY, ZZ	YY, ZZ		XX, YY, ZZ	XX, YY	XX, YY, ZZ	XX, YY	XX, YY, ZZ	XX, YY, ZZ	XX, YY, ZZ	XX, YY
YXYX	XX, YY, ZZ	XX, ZZ	XX, YY	XX, YY, ZZ		ZZ	XX, YY	ZZ	YY, ZZ	XX, YY, ZZ	XX, YY	XX, YY, ZZ
YXYX-CPMG	XX, ZZ	XX, ZZ	XX, YY, ZZ	XX, YY	ZZ		ZZ	XX, YY	YY, ZZ	YY, ZZ	XX, YY, ZZ	XX, YY
YXYX	XX, ZZ	XX, YY, ZZ	XX, YY	XX, YY, ZZ	XX, YY	ZZ		ZZ	XX, YY, ZZ	YY, ZZ	XX, YY	XX, YY, ZZ
YXYX-CPMG	XX, ZZ	XX, ZZ	XX, YY, ZZ	XX, YY	ZZ	XX, YY	ZZ		YY, ZZ	YY, ZZ	XX, YY, ZZ	XX, YY
YY	XX, YY	XX, YY, ZZ	XX, YY, ZZ	XX, YY, ZZ	YY, ZZ	YY, ZZ	XX, YY, ZZ	YY, ZZ		XX, ZZ	XX, ZZ	XX, ZZ
YY-CPMG	XX, YY, ZZ	XX, YY	XX, YY, ZZ	XX, YY, ZZ	XX, YY, ZZ	YY, ZZ	YY, ZZ	YY, ZZ	XX, ZZ		XX, ZZ	XX, ZZ
YYYY	XX, YY, ZZ	XX, YY, ZZ	XX, YY	XX, YY, ZZ	XX, YY	XX, YY, ZZ	XX, YY	XX, YY, ZZ	XX, ZZ	XX, ZZ		XX, ZZ
YYYY-CPMG	XX, YY, ZZ	XX, YY, ZZ	XX, YY, ZZ	XX, YY	XX, YY, ZZ	XX, YY	XX, YY, ZZ	XX, YY	XX, ZZ	XX, ZZ	XX, ZZ	

XX , YY or ZZ couplings.

This matrix is not intended to be comprehensive, but to provide a reference for the simplest sequences and static couplings that can be eliminated. Other hardware platforms may have additional native pulses available, or more complex types of couplings. Furthermore, we have limited ourselves to decoupling sequences that form an identity - they can be inserted into the circuit without additional compiling. However, we note that if we drop this requirement, a wider range of sequences is available. This may be more practical than it first appears, as NISQ circuits are often formed of alternating layers of 1Q and 2Q gates, where the 1Q layers can express any $U(2)$ rotation. As discussed, a common source of idle time is during nearby 2Q gates, meaning that the idle qubits will have a fully expressive $U(2)$ rotation on either side of the idle time. This opens up the possibility for non-identity sequences that can target a wider variety of couplings, with potentially fewer pulses. The correction to the identity needs to only be compiled into the following 1Q layer. Below, we outline an approach to generating such sequences.

For the purpose of dynamical decoupling, we can also express the constant interaction between qubits using superoperator representation. For simplicity, let's assume the crosstalk between qubits can be modeled by a constant Hamiltonian H [41]. Any Hamiltonian for a two-qubit system can be represented using 16 Pauli operators, i.e. $\{I, X, Y, Z\}^{\otimes 2}$. In this basis, the constant ZZ cross-talk is the vector $v = (0, \dots, 0, 1)$. In dynamical decoupling, we usually consider π or $\pi/2$ pulses, which are native pulses on superconducting hardware. Therefore, we can work with a subspace that is closed under the action of all the available

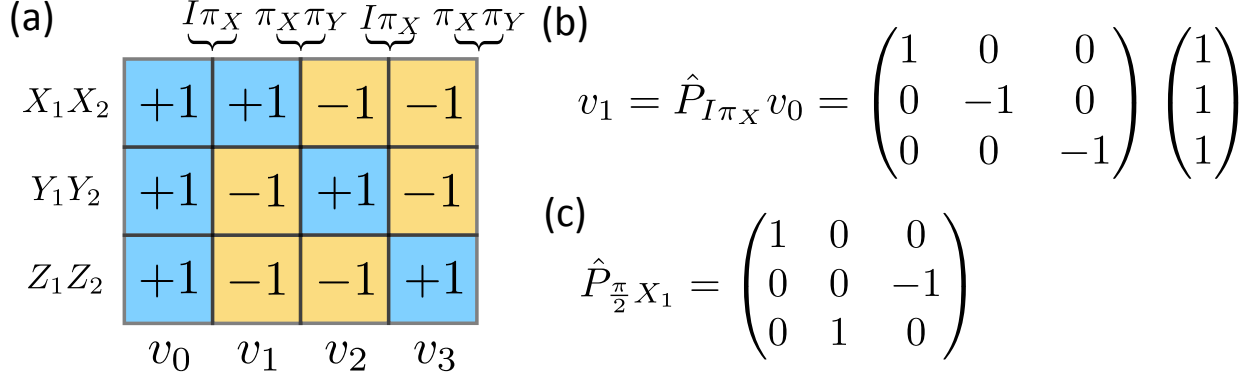


FIG. 6: Matrix representation of pulses in Pauli basis.

pulses. If the crosstalk between two qubits is instead modeled by the Heisenberg interaction, i.e., $H = X_1X_2 + Y_1Y_2 + Z_1Z_2$, and only π pulses are available, the subspace spanned by X_1X_2 , Y_1Y_2 and Z_1Z_2 is closed under the π pulses. And the representation of π pulses will be diagonal matrices. In Fig. 6 (a), the initial Hamiltonian is represented by vector v_0 , which is the first column. A π_X pulse on the second qubit is represented as the 3-by-3 matrix in Fig. 6 (b) to get the updated vector representation v_1 . And if four pulses are allowed per unit time, the concatenation of $[v_0; v_1; v_2; v_3]$ as shown in Fig. 6 (a) is also called toggling-frame sequence representation [42]. Suppose we choose a sequence of pulses $\hat{P}_1, \dots, \hat{P}_L$, at time $\Delta t, \dots, L\Delta t$. The time-averaged Hamiltonian would be $\bar{v} = \Delta t \sum_{l=0}^L v_l$, where $v_l = \prod_{i=1}^l \hat{P}_i v_0$. If the time window between different pulses is not uniform, then $\bar{v} = \sum_{l=0}^L v_l \Delta t_l$. The goal of dynamical decoupling is to let $\bar{v} = \vec{0}$. In other words, the summation of each row in the Fig. 6 (a) is zero. Using the superoperator and toggling-frame representation, one can transfer the DD sequence design problem into a discretized optimization problem.

By converting the design of the DD sequence into a discrete optimization, we have found several novel DD sequences for different types of qubit crosstalk. Some DD sequences with only π -pulses together with interaction Hamiltonians are listed below.

- $H = X_1X_2 + Y_1Y_2 + Z_1Z_2$:
 $I\pi_x \rightarrow \pi_x\pi_y \rightarrow I\pi_x \rightarrow \pi_x\pi_y$
- $H = X_1X_2 + Y_1Y_2 + Z_1Z_2 + Z_1 + Z_2$:
 $\pi_x I \rightarrow I\pi_y \rightarrow I\pi_y \rightarrow \pi_y\pi_x \rightarrow \pi_x I \rightarrow \pi_y\pi_x \rightarrow I\pi_y \rightarrow I\pi_y$
- $H = X_1X_2 + Y_1Y_2 + Z_1Z_2 + Z_1 + Z_2 + X_1 + X_2$:

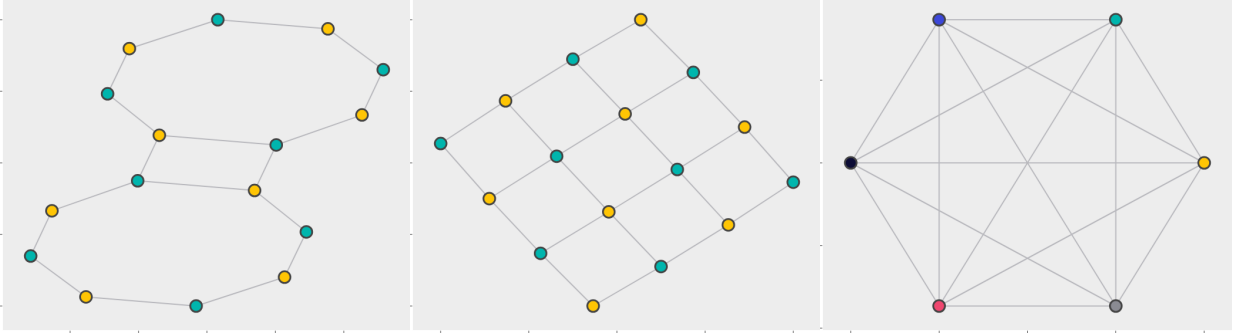


FIG. 7: The coloring of the (a) Aspen lattice, (b) square lattice, (c) fully-connected lattice. For the Aspen and square topologies, two syncopated sequences are sufficient to decoupling all the qubits. For the fully-connected model, however, each qubit requires a sequence.

$$\pi_y \pi_z \rightarrow \pi_y \pi_x \rightarrow \pi_y \pi_x \rightarrow \pi_y \pi_z \rightarrow \pi_y \pi_x \rightarrow \pi_y \pi_z \rightarrow \pi_y \pi_z \rightarrow \pi_y \pi_x$$

- $H = X_1 X_2 + Y_1 Y_2 + Z_1 Z_2 + Z_1 + Z_2 + Y_1 + Y_2 + X_1 + X_2 :$

$$\begin{aligned} \pi_y \pi_z \rightarrow \pi_x \pi_y \rightarrow \pi_y \pi_z \rightarrow \pi_y \pi_z \rightarrow \pi_y \pi_z \rightarrow \pi_x \pi_y \rightarrow \pi_y \pi_z \rightarrow \pi_y \pi_z \rightarrow \pi_y \pi_z \rightarrow \pi_x \pi_y \rightarrow \\ \pi_y \pi_z \rightarrow \pi_x \pi_y \end{aligned}$$

With $\pi/2$ -pulses, the length of DD sequences could be potentially reduced.

1. Syncopation on a crosstalk graph

Qubits are typically laid out in a lattice topology with nodes representing the physical qubits and edges representing interactions between them. Interactions make entangling gates possible, but are frequently the source of static crosstalk, as is the case in the Aspen architecture, but crosstalk is not limited to the physical topology and may also occur through other mechanisms. Regardless, given a proposed set of crosstalk relationships forming a graph, we can ask how to select a set of decoupling sequences such that the crosstalk is maximally suppressed. This amounts to solving the graph-coloring problem on the crosstalk graph, where each color is a decoupling sequence which syncopates with every other sequence (color). The number of required sequences is the chromatic number of the graph.

While on the Aspen architecture know the source and approximate magnitude of the fixed static couplings, it could be the case that in other architectures or more advanced

designs we have no prior knowledge of static couplings. Thus, we propose that expanding on Section III A, carefully selected patterns of syncopation could be used to identify unknown crosstalks. Using Table II, it is possible to select sequences which eliminate some crosstalks while preserving others, allowing a crosstalk model to be iteratively constructed from the measurement of many decoupling patterns. Hamiltonian engineering of this nature was further explored in refs [43] and [44].

Theorem 1. *Finding the upper bound of minimal dynamical decoupling sequence patterns for qubits with interaction represented by an arbitrary graph is NP-Complete.*

Proof. Let a graph $G(V, E)$ represent the cross-talk between qubits, where each vertex $v \in V$ is a qubit, and an edge $e \in E$ represents cross-talk between them. And label each dynamical decoupling pattern on a single qubit with a different color. Different colors on two connected vertices can cancel the cross-talk. Then, the minimal number of colors needed to color the vertices without any two connected nodes having the same color is the minimal number of dynamical decoupling sequence patterns to cancel all the cross-talks. This number is also called chromatic number $\chi(G)$ of a graph. Since finding the chromatic number of a graph is NP-Complete [45], that concludes the proof. \square

Corollary 1.1. *The minimal length of the syncopated dynamical sequence needed to cancel all the ZZ-type cross-talk is $2^{\chi(G)}$, where G is the graph representation of the crosstalk, and $\chi(G)$ is the chromatic number of the graph G .*

Appendix D: Determining g

The combination of Ramsey measurements and decoupling sequences we have described provides a highly accurate way to measure the coupling between a pair of qubits. In order to validate the experimental result from the main text, an alternative approach for obtaining g is described based on the two-qubit gate physics.

Each coupled pair of qubits consists of a tunable-frequency qubit and a fixed-frequency qubit coupled by a transverse coupling, gXX . In the weakly-coupled limit in which the qubits are operated, this becomes an effective ZZ coupling. We refer readers to [30] for a full treatment.

The two-qubit gate is activated by the condition

$$\hat{H}_{int} = g \sum_{n=-\infty}^{\infty} J_n\left(\frac{\omega_T}{2\omega_p}\right) e^{i(2n\omega_p t + \beta_n)} \times \left\{ e^{-i\Delta t} |10\rangle\langle 01| + \sqrt{2} e^{-i(\Delta + \eta_F)t} |20\rangle\langle 11| + \sqrt{2} e^{-i(\Delta - \eta_T)t} |11\rangle\langle 02| \right\} \quad (D1)$$

Where J_n is the n^{th} Bessel function of the first kind, Δ is the detuning and β_n is the phase.

$$\Delta = \bar{\omega}_T(\tilde{\Phi}) - \omega_F \quad (D2)$$

$$\beta_n = (\tilde{\omega}_T / \omega \omega_p) \sin(2\theta_p) + (2\theta_p + \pi)n \quad (D3)$$

We can see the Hamiltonian produces three resonance conditions.

$$2n\omega_p = \Delta(\tilde{\Phi}) \rightarrow |10\rangle \leftrightarrow |01\rangle \quad (D4)$$

$$2n\omega_p = \Delta(\tilde{\Phi}) - \eta_T \rightarrow |11\rangle \leftrightarrow |02\rangle \quad (D5)$$

$$2n\omega_p = \Delta(\tilde{\Phi}) + \eta_T \rightarrow |11\rangle \leftrightarrow |20\rangle \quad (D6)$$

Each resonance has an effective coupling strength $g_{eff}^{(n)}$ which determines the Rabi frequency and the resonant linewidth of the interaction at the n^{th} harmonic. This is given by the time-independent prefactor for each term in the Hamiltonian:

$$g_{eff}^{(n)} = g J_n\left(\frac{\tilde{\omega}_T}{2\omega_p}\right) \leftarrow i\text{SWAP} \quad (D7)$$

$$g_{eff}^{(n)} = \sqrt{2} g J_n\left(\frac{\tilde{\omega}_T}{2\omega_p}\right) \leftarrow i\text{CZ} \quad (D8)$$

A parametric drive that resonantly couples two levels produces swapping in the subspace of those two levels, described by

$$\hat{U} = \begin{pmatrix} \cos(\theta/2) & i e^{-i\phi} \sin(\theta/2) \\ i e^{i\phi} \sin(\theta/2) & \cos(\theta/2) \end{pmatrix} \quad (D9)$$

where the population exchange, θ is given by

$$\theta = 2 \int_0^\tau g_{eff}(t) dt \quad (\text{D10})$$

Thus, g_{eff} can be straightforwardly determined from the iSWAP gate time. In the case of qubits 101 and 102, the iSWAP time is 160ns, which corresponds to a g_{eff} of 1.56 MHz. The modulation frequency is 519.23 MHz, corresponding to a AC flux amplitude of $0.602 \Phi_0$.

The re-normalization constant, r is thus

$$r = J_n\left(\frac{\tilde{\omega}_T}{2\omega_p}\right) = 0.135 . \quad (\text{D11})$$

This corresponds to a g of 12.42 MHz, which is in close agreement with the value determined via the dispersive shift (11.3 Mhz).